
1 Tailoring the Physical Properties of Graphene

*C. G. Rocha, M. H. Rummeli, I. Ibrahim,
H. Sevincli, F. Börrnert, J. Kunstmann,
A. Bachmatiuk, M. Pötschke, W. Li,
S. A. M. Makharza, S. Roche, B. Büchner,
and G. Cuniberti*

CONTENTS

1.1	Introduction	1
1.2	Basic Electronic Properties of Graphene-Based Structures	2
1.2.1	Graphene Nanoribbons	4
1.3	Edge Disorder in Graphene Structures	6
1.4	Vibrational Properties and Thermal Properties	8
1.5	Mechanical Properties of Graphene	10
1.6	Graphene's Transport Properties under External Fields	11
1.7	Magnetic Properties of Graphene	14
1.8	Synthesis of Graphene	15
1.9	Graphene and Some of Its Applications	16
	References	17

1.1 INTRODUCTION

For many years graphene was deemed an “academic” material where its perfect honeycomb monolayer structure of carbon atoms was treated solely as a theoretical model for describing the properties of various carbon-based materials such as graphite, fullerenes, and carbon nanotubes. Older theoretical predictions [1,2,3], studying pristine two-dimensional (2D) crystals, presumed graphene would be unstable in reality due to thermal fluctuations that prevent long-range crystalline order at finite temperatures. This presumption was strongly supported by various experimental investigations with thin films in which the samples became unstable as their thickness was reduced. Now, early in the twenty-first century, graphene has emerged as a real sample [4,5]. The initial works by Geim and Novoselov showed the isolation of astonishingly thin carbon films and eventually monolayer graphene by simply using scotch tape. Since its discovery, the variety of physical phenomena explored using graphene has expanded at a remarkably fast pace inspiring a wide variety of novel technological applications. Spurred on by potential future applications

like single-electron transistors [6], flexible displays [7,8], and solar cells [9], a lot of research effort is being devoted to understanding the main physical properties of graphene. For this reason, the following subsections of this review aim to introduce the reader to the basic features of graphene, in particular, its unique electronic structure and related electrical transport properties. Later, the state of the art regarding other important physical aspects of graphene beyond its electrical properties is also reviewed including its mechanical, magnetic, and thermal properties.

1.2 BASIC ELECTRONIC PROPERTIES OF GRAPHENE-BASED STRUCTURES

Graphene is defined as a single layer of carbon atoms arranged in a hexagonal lattice, as illustrated in Figure 1.1a. Its atomic structure can also be used as a basic building block to construct other carbon-based materials: (1) it can be folded into fullerenes, (2) rolled up into nanotubes, or (3) stacked into graphite. The primitive cell of graphene is composed of two non-equivalent atoms, A and B, and these two sublattices are translated from each other by a carbon-carbon distance $a_{c-c} = 1.44 \text{ \AA}$.

A single carbon atom has four valence electrons with a ground-state electronic shell configuration of $[\text{He}] 2s^2 2p^2$. In the case of graphene, the carbon-carbon chemical bonds are due to hybridized orbitals generated by the superposition of $2s$ with $2p_x$ and $2p_y$ orbitals. The planar orbitals form the energetically stable and localized σ -bonds with the three nearest-neighbor carbon atoms in the honeycomb lattice, and they are responsible for most of the binding energy and for the elastic properties of the graphene sheet. The remaining free $2p_z$ orbitals present π symmetry orientation and the overlap of these orbital states between neighboring atoms plays a major role in the electronic properties of graphene. For this reason, a good approximation for describing the electronic structure of graphene is to adopt an orthogonal nearest-neighbor tight-binding approximation assuming that its electronic states can

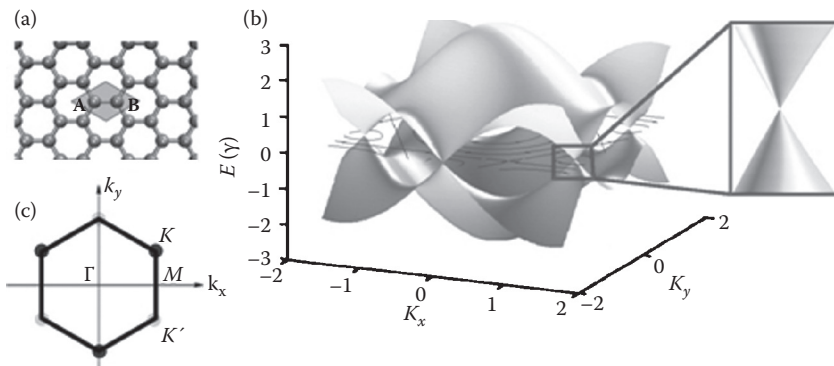


FIGURE 1.1 (See color insert.) (a) Honeycomb lattice of graphene. The shadowed area delineates the unit cell of graphene with its two nonequivalent atoms labeled by A and B. (b) Band energy dispersion obtained via tight binding approximation. The inset highlights the conical-shape dispersion around the charge neutrality point. (c) First Brillouin zone.

be simply represented by a linear combination of $2p_z$ orbitals. Solving the Schrödinger equation, which reduces into a matrix secular expression, one can obtain the energy dispersion relation of π (bonding) and π^* (antibonding) bands [10,11,12].

$$E(k_x, k_y) = \pm \gamma \sqrt{1 + 4 \cos\left(\frac{\sqrt{3}k_x a}{2}\right) \cos\left(\frac{k_y a}{2}\right) + 4 \left[\cos\left(\frac{k_y a}{2}\right)\right]^2} \quad (1.1)$$

where k_x and k_y are the components of the k vector that are folded onto the first hexagonal Brillouin zone (shown in Figure 1.1c) and $\gamma = 2.75$ eV is the hopping energy. The electronic structure of graphene can also be represented by closed-form expressions obtained analytically for the single-electron propagators written on a real-space basis [13]. In Figure 1.1b, one can see the band structure of graphene obtained from such a simple tight-binding model, which yields symmetric conduction and valence bands with respect to the Fermi energy (also called the *charge neutrality point* or *Dirac point*) set at 0 eV. Graphene valence and conduction bands are degenerate at 6 points located on the corners of the Brillouin zone, also called K and K' valleys. The hexagonal region (Brillouin zone) has a side length of $4\pi/3a$ and delineates the Fermi surface of the graphene as shown in Figure 1.1c. Since the Fermi surface of graphene is compacted to a zero dimension zone composed of a finite set of 6 points on its Brillouin zone, graphene is usually termed a *semimetal* material with no overlap or zero-gap semiconductor. It is easy to see that the electronic properties of graphene are invariant by interchanging the K and K' states, which means that the two valleys are related by time-reversal symmetry. Fascinating physical phenomena can be unveiled while attempting to break this effective time-reversal symmetry.

The low-energy dispersion near the valleys exhibits a circular conical shape, as displayed in the inset of Figure 1.1b, unlike the quadratic energy–momentum relation obeyed by electrons at the band edges in conventional semiconductors. Comparing this linear energy relation of graphene with the dispersion of massless relativistic particles obtained from the Dirac equation, one can see that graphene charge carriers can behave as Dirac fermions with an effective Fermi velocity that is around 300 times smaller than the speed of light [5]. This makes graphene a reliable system to study quantum electrodynamic phenomena, an area of investigation previously limited to particle physics and cosmology investigations. In this sense, several research groups have already addressed a variety of unusual phenomena that are revealed by graphene materials, which are characteristic of Dirac relativistic particles, for instance, the absence of localization effects even when disorder elements can take place [14,15], robust metallic conductivity even in the limit of nominally zero carrier concentration, and the half-integer quantum Hall effect.

Additional band features can be learned from the energy spectrum of graphene when the adopted model goes beyond the simple orthogonal tight-binding approach or Dirac formalism. More robust techniques, such as *ab initio* methods, predict that antibonding bands are located at a higher energy with respect to the bonding states if the overlapping integral matrix is nonorthogonal [16]. Sophisticated implementations for single- π band tight binding schemes considering up to the third-nearest

neighbor interactions and overlap elements can result in an accurate description of the electronic properties in relation to first principle calculations [17].

The amazing electronic properties of graphene have greatly motivated the scientific community to pursue a better understanding of their main physical features with the bonus of converting them into real technological applications. However, the absence of an energy band gap greatly restricts its use on digital devices. Thus, alternative strategies capable of inducing a band gap in graphene are being sought. Several strategies have already been successfully adopted to modify the electronic structure of graphene and include chemical doping, interaction with substrates, and the application of mechanical forces or external electric/magnetic fields. Stacked graphene layers in the form of bilayers or graphite structures [18,19,20] also offer a promising route for band gap manipulation. Advanced lithographic techniques [21] employed to tailor wide graphene samples into nanoscale structures have shown that lateral confinement of charge carriers can work as an efficient energy gap-tuning parameter. Such narrow graphene structures are known as *graphene nanoribbons* (GNR) and it has been demonstrated that their energy gap scales inversely with the width. The following section is dedicated to a review of the main physical properties of such confined graphene systems.

1.2.1 GRAPHENE NANORIBBONS

Besides the idealizations of graphenelike 2D membranes, atomistic models of thin graphene strips were also addressed primarily to investigate the nature of edge dislocations and the appearance of defective dangling bonds in carbon networks [22]. Such narrow graphene strips, known as graphene nanoribbons, were also not expected to exist in nature. The discovery that graphene materials can be fabricated in the free state and combined with modern lithography techniques has confirmed that confined graphene structures are experimentally feasible. Currently, the synthesis of graphene nanoribbon samples has advanced considerably beyond that possible with conventional lithographic methods. For instance, “ribbons” with widths smaller than 10 nm have been synthesized via crystallographic etching [23,24], sonochemical techniques [25], and even through the unzipping of carbon nanotubes [26–28]. An original fabrication process for graphene nanoribbons with atomic-scale precision has recently been realized through the controlled assembly of molecular precursors consisting of polycyclic aromatic hydrocarbon compounds [29].

The physical properties of graphene nanoribbons are highly dependent on their width and the topology of the edge structures. There are two canonical types of graphene edges, referred to as *armchair* (AGNR) and *zigzag* (ZGNR) ribbons, and examples of their atomic structure can be seen in Figure 1.2. The atoms located on the edges are highlighted in green and W denotes the width of the ribbon. The width of an armchair ribbon can be defined in terms of the number of dimer lines: $W_a = (N_a - 1)a/2$ for armchair ribbons and $W_z = (N_z - 1)\sqrt{3}a/2$ for zigzag ribbons; N_a and N_z are their respective number of carbon chains.

The electronic structure of graphene nanoribbons can be represented in a simple manner following a single- π band tight binding description or Dirac approach where “particle-in-a-box” boundary conditions are applied to the ribbon’s terminations. In

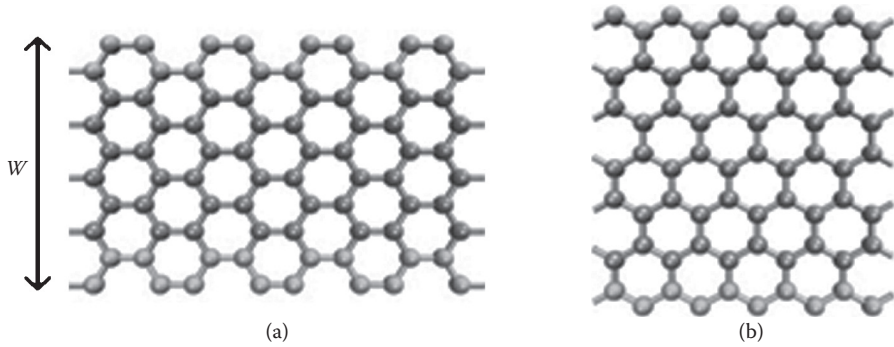


FIGURE 1.2 (See color insert.) Atomic structure of an (a) armchair- and a (b) zigzag- edge graphene nanoribbon. Green color atoms delineate the respective edge-shape and W denotes the width of the ribbon.

this case, the wave vector components lying in the width direction will be quantized, whereas those parallel to the axial direction remain continuous for infinite systems. In other words, limiting the width of a *bulk* graphene sheet means “slicing” the energy band structure of Figure 1.1b in well-defined directions; their projections can be seen on the Fermi surface as presented on the top panels of Figure 1.3. The quantization lines correspond to the allowed k states for three distinct graphene nanoribbons—AGNR(8), AGNR(9), and ZGNR(8)—placed over graphene’s Brillouin zone. Whenever one of these states crosses one of the graphene’s valleys, valence and conduction bands touch each other at the Fermi level and the ribbon exhibits metallic behavior, otherwise it is semiconducting [30].

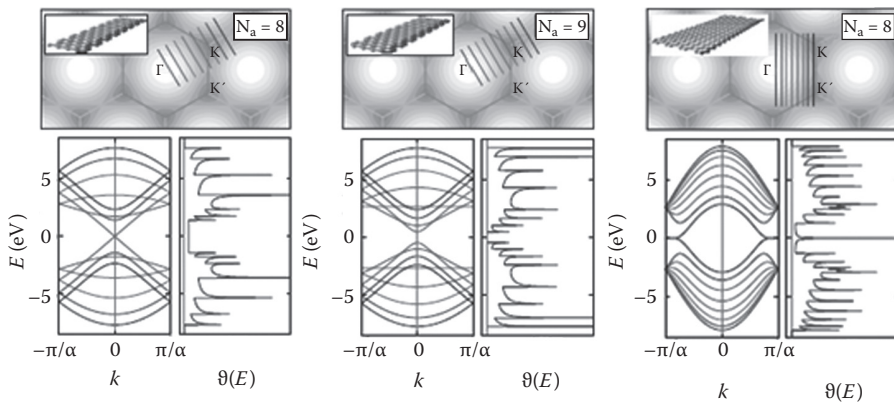


FIGURE 1.3 (See color insert.) (Top panels) Zone-folding diagram for three different graphene nanoribbons: left, AGNR(8); middle, AGNR(9); and right, ZGNR(8). The parallel lines in the Brillouin zone represent the allowed quantized states of the ribbon projected in momentum space. Their respective energy band structures and density of states curves are displayed on the lower panels. (Adapted from N. Nemeč, Quantum transport in carbon-based nanostructures. Dr. rer. nat. (equiv. PhD) thesis, University of Regensburg, September 2007.)

Their respective energy dispersion relation and density of states curves calculated via nearest-neighbor tight-binding approximation are also shown in the lower panels. According to this simple description, one can predict that zigzag ribbons of any width show a singular edge state that decays exponentially into the center of the ribbon. Such edge states are twofold degenerate at the Fermi energy and reveal a nondispersive feature that lasts about $1/3$ of the total size of the graphene Brillouin zone. As a consequence, the density of states of zigzag ribbons is characterized by a pronounced peak located at the charge neutrality point. Although there are still controversies concerning the associated energy eigenvalue of the edge state, the detection of such a peak has been accomplished through scanning tunneling microscopy measurements performed near zigzag edge sections of graphite [31]. In stark contrast, no such localized state appears in nanoribbons having an armchair edge configuration. Moreover, this simple model shows that armchair ribbons can change their electronic character depending on their width. An armchair nanoribbon can behave as a metal when the number of atoms along its width is equal to $3j + 2$, where j is an integer. This class of armchair ribbons exhibits semiconducting behavior when more sophisticated electronic structure models are applied or the edge atoms are parameterized to include the effects of hydrogen passivation. The remaining armchair ribbons in the $3j$ and $3j + 1$ categories are all semiconductors independent of the adopted model [22].

The challenge of inducing a band gap in graphene seems to be solved by cutting it into ribbons. On the other hand, the edges bring additional problems. Graphene nanoribbons indeed possess a band gap, but their edges have inherent edge disorder [32]. It turns out that their electronic properties are strongly reliant on the topological details of the atoms located on their extremities. Roughness, or even chemical groups bound to the edges, can also affect the electronic features of the ribbons. In this sense, studies focusing on disorder effects in graphene structures are of extreme relevance for envisioning the main mechanisms behind their electronic response.

1.3 EDGE DISORDER IN GRAPHENE STRUCTURES

The dominant scattering processes and resulting transport features of graphene are very dependent on the range of the disorder potential and the robustness or destruction of the underlying sublattice symmetries. A variety of physical behaviors can be unveiled when short-range interactions take place in graphene since all possibilities of intravalley and intervalley scattering events between K and K' points are allowed. Short-range potentials formed, for instance, by atomically sharp defects such as vacancies [33,34]; Anderson disorder or edge deformations induce chirality breaking, leading to strong backscattering events and localization effects. In particular, graphene nanoribbons are naturally subjected to edge disorder due to the high reactivity of edges that can be subjected to chemical passivation, roughness, and structural reconstruction [35]. In addition, confinement effects are expected to maximize the sensitivity of the structures regarding the presence of disorder. Joule heating techniques capable of vaporizing carbon atoms from the edges has been carefully employed to pattern the morphology of nanoribbon extremities. The successful stabilization of sharp edge reconstructions mostly formed with either zigzag or armchair

configurations has been observed [36]. Nonetheless, improving the quality of the edge-shapes in practice remains a difficult task. A multitude of different edge topologies have been characterized and so researchers must cope with a vast physical scenario involving prominent localization effects induced by edge disorder [25,37,38].

Depending on the edge shape of the graphene structure, different band gaps for similarly sized systems can be generated since its electronic structure is greatly influenced by disorder. Transport measurements realized in etched graphene samples have demonstrated that sharp resonances can appear inside the transport gap, providing evidence that the atomic details of tailored graphene systems play an important role in their conducting properties [39]. Atomistic models for edge disorder are often used to investigate the impact of topological edge roughness on the conducting properties of the ribbons. The boundaries are initially assumed to be perfect. Subsequently, the erosion of the edges can be simulated by randomly setting the hopping elements of neighboring atoms to zero or setting their onsite energies to very high values. The calculations indicate that even when very weak edge disorder effects are simulated, a prominent modification in the conductance profile of the nanoribbons is obtained [40,41]. In Figure 1.4, the impact on the conductance of a zigzag-edge ribbon considering different complexities for the edge disorder is

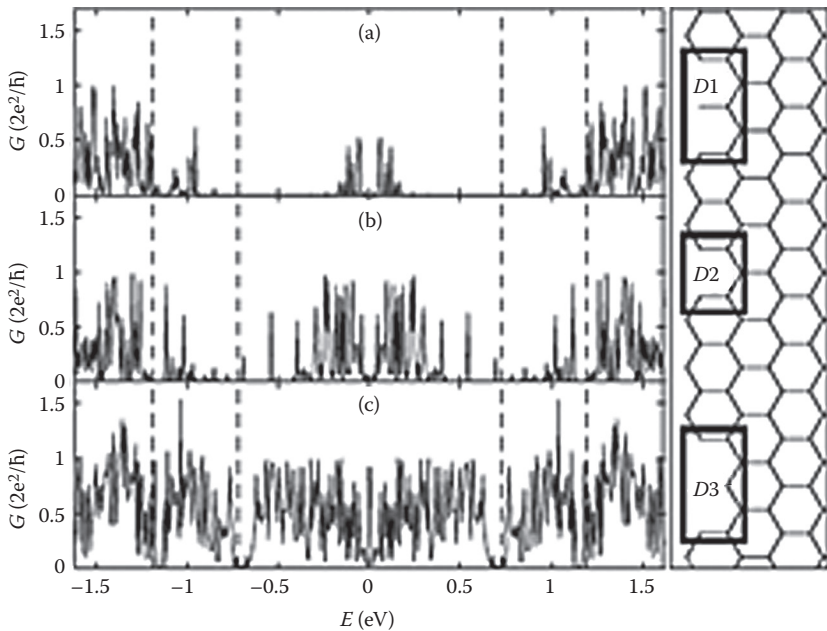


FIGURE 1.4 (Left panels) Conductance as a function of energy obtained from a disordered ZGNR(16) with length $L = 500$ nm and imposing a probability of 7.5% for removing carbon atoms from the edges. (Right panels) Schematic pictures representing the different types of defects: (D1) is an example of the Klein defect and (D2) and (D3) correspond to the defects where one and two hexagons, respectively, are missing. (Adapted from A. Cresti and S. Roche. 2009. Edge-disorder-dependent transport length scales in graphene nanoribbons: From Klein defects to the superlattice limit. *Physical Review B* 79: 233404-1-4.)

shown [35]. The D1 defect is known as the Klein defect and is composed of a zigzag edge with a single carbon bound on the edges [42,43]. The D2 and D3 imperfections consist of withdrawing one or two consecutive hexagons from the edges. The atoms were randomly removed with an equal probability of 7.5% and length of the scattering region is $L = 500$ nm. The conductance around the charge neutrality point is highly suppressed especially in the presence of Klein and D2 defects. A few resonance peaks survive within the energy range where one conductive channel was active regardless of whether the defects were absent or not. A robust conducting profile is observed when D3 defects exist, suggesting that the system can evolve from a quasiballistic to a localized regime depending on the details of the defects and as the length of the scattering region increases.

Similar studies performed in disordered armchair ribbons have shown that these later structures are relatively more sensitive to edge disorder in comparison to zigzag configurations. In other words, disordered armchair structures have a greater propensity to manifest localization effects. It was demonstrated that only 10% of edge defects are enough to wash out the electronic transmission in a wide range of energies of metallic armchair structures [44]. Specifically, for the case of semiconducting armchair ribbons, it has been shown that edge disorder is capable of transforming their electronic character into Anderson insulators as long as their width is kept relatively wide in order to minimize the impact of disordered edges. Insulating character is also achieved in ribbons with lengths large enough to avoid the direct tunneling of electrons along the channels [45,46].

The impact of the edges on the electronic structure of nanoribbons can be controlled by chemical passivation [47] where different species could, in principle, react with the carbon atoms situated on the extremities rather than the commonly used hydrogen saturation. In reality, not only the edges of the ribbons can be thought of as the most energetic location for dopants. The specific topology of nanoribbon edges enters as an additional control parameter for the segregation of impurities across their width and their distribution can be tuned by gate potentials [48]. Such studies involving doping processes in graphene nanoribbons open a wide field of applications in the industry of chemical and biosensor devices.

In addition to such amazing electronic properties, graphene structures are also exceptional materials for transferring heat [49,50]. The investigation involving heat conductivity can favor the elaboration of effective heat-dissipating devices in order to cool down electronic components. In addition, the variety of phenomena explored using graphene increased after its confirmation as the strongest and lightest material ever to be measured. The next sections are devoted to discussing the main achievements in the field of heat conductivity, thermal vibrations, and mechanical properties in graphene structures.

1.4 VIBRATIONAL PROPERTIES AND THERMAL PROPERTIES

At room temperature (RT), the thermal conductivity (κ) of single-layer graphene is mostly due to acoustic phonons [51]. The high value of κ is attributed to the absence of crystal defects, and suppression of Umklapp processes as the number of layers is

reduced [52], that is, long mean-free paths of phonons. Such high values suggest that graphene can play a key role in future nanoelectronic devices [53].

The phonon branches of graphene can be grouped as in-plane (LA, TA, LO, and TO) and out-of-plane (flexural) modes (ZA and ZO). The acoustic flexural mode (ZA) in two-dimensional crystals has a quadratic dispersion in the vicinity of the Γ point of the Brillouin zone, and exhibits a singularity in the density of states at zero energy. At finite temperatures, thermal fluctuations are expected to give rise to atomic displacements as large as the interatomic distance; therefore low-dimensional crystals should be unstable [1,2]. However, macroscopic samples of graphene are shown to be stable and preserve their crystal quality, which is believed to be due to the existence of microscopic crumpling in the third dimension [54].

The ballistic thermal conductivity of graphene is isotropic [51]. In the temperature range below 20 K, the ZA mode is detrimental to conduction. Above 20 K, the LA and TA modes also contribute, however the ZA mode dominates the thermal conduction. The exact solution of the phonon Boltzmann equation shows that the ZA mode is the dominant heat carrier at higher temperatures as well [55]. It is also shown that anharmonic scattering is significantly restricted for the flexural modes due to selection rules, and this behavior is robust to inclusion of ripples and isotopic impurities. There is a variety of values reported for κ of single-layer suspended graphene at room temperature ranging from 600 to 5000 $\text{Wm}^{-1}\text{K}^{-1}$ [49,56,57]. The disagreement needs to be clarified.

On the other hand, when graphene lies on a supporting substrate, phonons leak across the interface and the flexural modes are scattered strongly. Nonetheless, κ of graphene on SiO_2 substrate has been measured as 600 $\text{Wm}^{-1}\text{K}^{-1}$ at RT, considerably higher than that of copper [50,58]. The reduction of κ due to a supporting substrate also points to the interplay between the phonon scattering mechanisms and the number of graphene layers. Measurements on few-layer graphene, with the number of layers ranging between 2 and 10, shows the dimensional crossover from two dimensions to bulklike behavior, and the crossover is assigned to the intralayer coupling of low-energy phonons and enhanced Umklapp scatterings [52]. As a result, κ drops from 2800 to 1300 $\text{Wm}^{-1}\text{K}^{-1}$ when the number of layers is increased from 2 to 4. In most device applications, graphene will be encased within dielectric materials, which will alter the thermal properties significantly. Measurements on single-layer graphene encased within SiO_2 show that the thermal conductivity is suppressed down to 160 $\text{Wm}^{-1}\text{K}^{-1}$, and for few-layer graphene it increases with the number of layers approaching the limit of in-plane κ for bulk graphite [59].

Similar to the electronic states in GNRs, only standing wave solutions are allowed perpendicular to the ribbon axis [60]. Therefore the wave vector is discrete in this direction, $q_{\perp,n} = n\pi/W$, where W is the ribbon width, and $n = 0, \dots, N - 1$. The phonon branches of GNRs can be interpreted to consist of six fundamental modes that correspond to the modes of graphene, and their $6(N - 1)$ overtones [61], except for the fact that there exist 4 acoustic modes in quasi-one-dimensional crystals. In the ballistic regime, the thermal conductance of pristine GNRs is predicted to display a power law T at low temperatures, ranging from 1 to 1.5, from narrow to wide

ribbons [51,62]. Since one has edges, it is unavoidable to have some irregularities in the edge shape and width of the GNRs. The effect of disorder in the edge shape of GNRs increases with decreasing ribbon width and suppresses thermal conductivity strongly for GNRs having widths of 20 nm and below [63,64]. The thermal conductivity of GNRs with sub-20-nm widths was measured as $\sim 1000 \text{ Wm}^{-1}\text{K}^{-1}$ in agreement with theoretical calculations [65,66].

1.5 MECHANICAL PROPERTIES OF GRAPHENE

Graphene received the title of “strongest material ever” after the confirmation of its sustaining breaking strengths of 42 N/m with an intrinsic mechanical strain of $\sim 25\%$ and Young’s modulus of $Y \sim 1.0 \text{ TPa}$ [67]. Its mechanical thickness can also be controlled as demonstrated through mechanical stress measurements performed on graphene sheets subjected to deformations induced by depositing different insulating capping layers [68]. The experimental findings regarding the main mechanical features of graphene have been confirmed by several theoretical works using different techniques. Among them, *ab initio* [69], tight binding [70], molecular dynamics simulations [71,72], and semiempirical models [73,74] have successfully estimated the Young’s modulus and other intrinsic mechanical quantities of graphene.

The outstanding mechanical properties of graphene have also attracted interest from electronic applications due to the potential use that these light, stiff, and flexible materials can offer for designing building-block components in nanoelectromechanical systems (NEMS). In particular, the fabrication of low-cost NEMS devices requires a complete correspondence between mechanical and electrical responses of the conductive channel. In this sense, the operation mechanism of an efficient NEMS based on graphene relies strictly on the feasibility of performing band gap engineering with the aid of external mechanical forces. Detailed analysis of the physical properties of uniaxially strained “graphene-bulk” has been widely studied by Raman spectroscopy [68,75,76] and suggests that manipulation of the band gap is possible. Nevertheless, most of these experiments were conducted on samples placed on top of flexible substrates, which can gradually stretch or bend the sheets. The pure electromechanical response of suspended 2D graphene is still under debate. According to several theoretical works, the electronic structure of suspended graphene is extremely resistant against mechanical forces, being able to support reversible elastic deformations above 20% [69,70].

Band gap engineering of strained graphene materials is possible when tailored structures, such as nanoribbons, are mechanically perturbed. It has already been shown that the transport and electronic features of graphene nanoribbons can be efficiently tuned as a function of strain [77–81]. These studies highlight important aspects of the synthesis of graphene-based molecular electromechanical devices [82]. The conductance of uniaxially stretched graphene nanoribbons is shown to be strongly dependent on their edge shape, as can be seen in Figure 1.5. Ribbons with armchair edge symmetry can undergo a metal–semiconductor transition as mechanical strain increases, whereas zigzag ribbons exhibit a more robust transport behavior against stretching. Very small strain values are sufficient to open an energy gap in

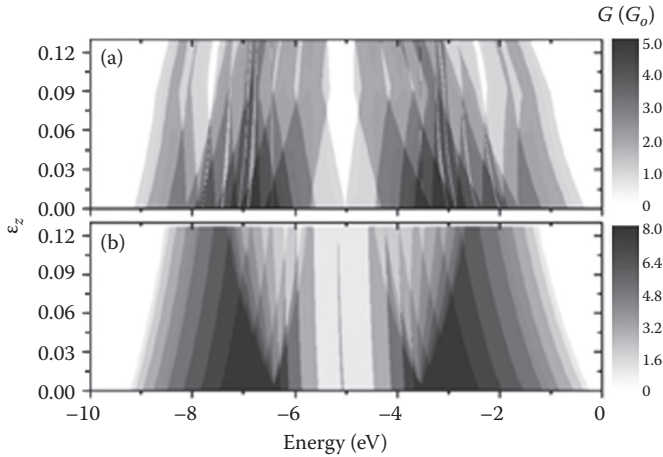


FIGURE 1.5 (See color insert.) Contour plots of conductance as a function of Fermi energy and mechanical strain for (top panel) an AGNR(11) and (lower panel) a ZGNR(10). (Adapted from M. Poetschke, C.G. Rocha, L.E.F. Foa Torres, S. Roche, and G. Cuniberti. Modeling graphene-based nanoelectromechanical devices. *Physical Review B* 81 (2010): 193404-1-4.)

AGNRs, confirming that their electronic character is sensitive to mechanical stress. In this sense, armchair edge ribbons are more suitable for engineering electromechanical devices in comparison to zigzag geometries.

1.6 GRAPHENE'S TRANSPORT PROPERTIES UNDER EXTERNAL FIELDS

The successful realization of graphene-based nanodevices depends mostly on patterning effective circuit architectures in which their electronic properties can be modified in a predetermined and reversible way. In fact, interesting quantum phenomena can be observed when the physical properties of low-dimensional systems are tuned by external fields such as electric or magnetic fields and gate voltages under dc conditions. Studies considering external fields in the stationary regime have been widely investigated both theoretically and experimentally. For instance, a graphene sheet experiencing the presence of a modulated electrical potential sustains strong modifications in its low-energy properties. The robust degeneracy at the Dirac point is split and the isotropic conelike structure of the energy relation is now composed of two distinct valley structures with highly anisotropic dispersions [83]. Theoretical investigations of graphene ribbons working as a transmission channel under transversal electric fields have demonstrated that the number of transmission modes can be controlled with the aid of an external voltage [84–86]. More importantly, the conductance of the system varies sharply by integer multiples of the quantum conductance with respect to the strength of the electric field. Additional transport features can be visualized when a rotating gate plate acts on the graphene ribbons. The transmission is shown to be dependent on the gate orientation and on the width of the ribbons [87]. External electric fields can also be used

to effectively tune important physical quantities of graphene such as work function [88] and electron–phonon coupling [89]. An efficient alignment tool was idealized by the application of external electric fields where the graphene membranes can be, in principle, oriented in particular directions in space via electric polarization effects [90]. Moreover, the electronic properties of graphene were finely tuned through the adsorption of molecules with strong electric dipole moments, capable of inducing a local electric field on the structures. Band gap engineering in graphene hosts was theoretically addressed by considering that the intensity of the external electric field can be controlled by means of the density of ad molecules [91]. An even wider set of electronic responses can be obtained from graphene nanostructures when a combination of both electric and magnetic fields is applied. Energy-gap modulation can be achieved in graphene nanoribbon channels exposed to fields oriented in a type of Hall configuration [92] as shown in Figure 1.6. The lowest and highest energy states of an initially semiconducting AGNR are shown to collapse at the Dirac point at a critical electric field, guiding the system toward a semimetallic arrangement. The competition between localization and delocalization effects generated by the respective magnetic and electric fields gives rise to a rich set of electronic responses that can certainly be implemented into promising electronic devices. Essentially, the fields induce a broad set of refinements in graphene’s energy spectrum such as $k \leftrightarrow -k$ symmetry breaking, drastic modification of low-energy dispersions, sub-band spacings, and edge states [93,94]. Furthermore, at a critical electric and magnetic field ratio, it has demonstrated that the Landau spectrum contracts, viz. the Landau energy level spacing, gradually decreases [95]. At the same time, electric

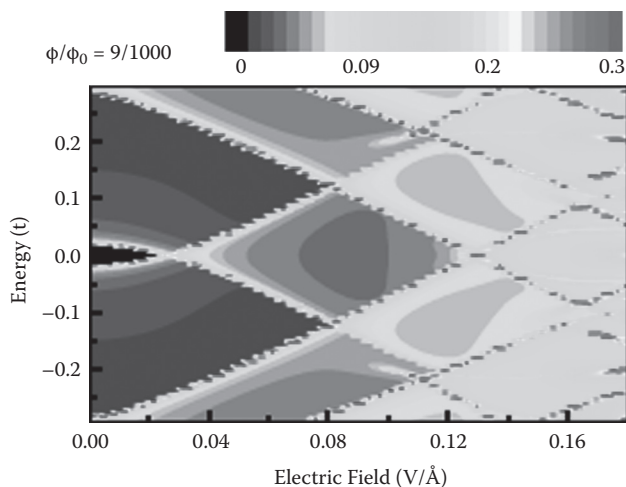


FIGURE 1.6 (See color insert.) Local density of states contour plot for a 24-AGNR as a function of the electric field intensity for a fixed magnetic flux of $\phi/\phi_0 = 9/1000$. Black corresponds to null density of states while the highest LDOS value is highlighted by red color. (Adapted from C. Ritter, S.S. Makler, and A. Latgé. Energy-gap modulations of graphene nanoribbons under external fields: A theoretical study. *Physical Review B* 77: 195443-1-5.; *Physical Review B* 82 (2008): 089903-1-2. With permission.)

excitations are found to disturb the magnetic susceptibility and the characteristic Haas-van Alphen oscillations observed in the magnetization curves calculated for graphene systems under magnetic fields [96]. Such anomalous phenomena are concluded to be associated with the relativistic flavor of the low-energy charge carriers in graphene.

Another possibility to control the electronic transmission of carbon-based nano-materials is through the use of time-dependent excitations [97]. Recent studies targeting the use of ac fields in graphene materials [98–100] shed light on this growing research area, often overshadowed by studies considering external fields in the stationary regime. Under ac signals, several theoretical works have highlighted graphene’s potential as a spectrometer device operating even at high-frequency noise. In particular, for the case in which a homogeneous ac gate can act on graphene channels, it has been shown that it is possible to achieve full control of the conductance patterns which, remarkably, resemble Fabry-Pérot interference patterns of light-wave cavities [98,101]. The results presented in Figure 1.7, obtained for an AGNR resonator, suggest several possibilities to tune the conductance profiles ranging from the standard dc regime (panel [a]), to suppression (panel [b]), phase change (panel [c]) of the oscillations, and robust behaviors (panel [d]) interpreted as a wagon-wheel effect held in the quantum domain. There is also an increasing interest in graphene’s photovoltaic Hall effect since it was confirmed that photo-induced dc currents can

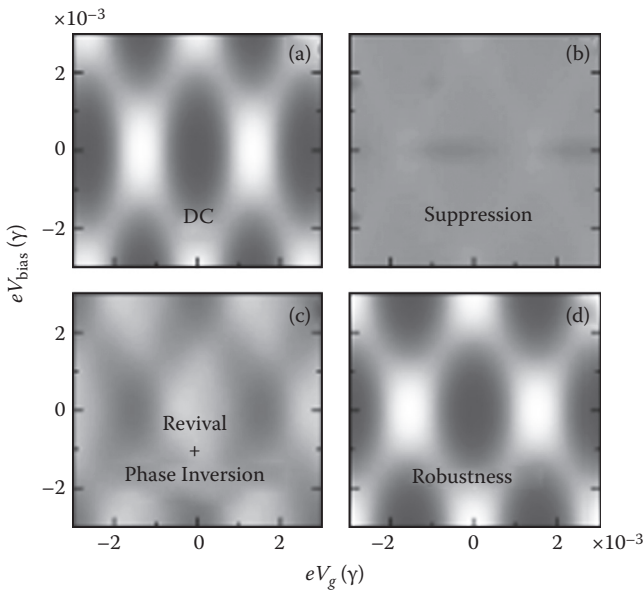


FIGURE 1.7 (See color insert.) Fabry-Pérot conductance interference patterns for an AGNR as a function of bias and gate voltages calculated for different driving frequencies and amplitudes associated with a time-dependent gate potential that follows a harmonic time dependency. White and dark blue colors correspond to maximum and minimum conductance values, respectively. (Adapted from C.G. Rocha, L.E.F. Foa Torres, and G. Cuniberti. Ac transport in graphene-based Fabry-Pérot devices. *Physical Review B* 81 (2010): 115435-1-8.)

be induced under intense light [102]. Such investigations underscore the potential for synthesizing organic solar cells based on graphene.

1.7 MAGNETIC PROPERTIES OF GRAPHENE

As discussed in Section 1.2.1, zigzag graphene nanoribbons have so-called edge states. According to numerous theoretical studies based on density functional theory or on the mean-field Hubbard model, it is believed that the associated peak in the density of states at the Fermi energy (E_F) gives rise to a magnetic instability, where the edge states become spin-polarized [22,103,104]. In the magnetic ground state, a band gap at E_F is opened, and the atoms are ferromagnetically ordered along one edge, and antiferromagnetically ordered between opposite edges. This antiferromagnetic ground state is consistent with the Lieb theorem for a biparticle lattice within a Hubbard model description [105]. The phenomenon of edge magnetism is not restricted to ideal ZGNRs but is believed to occur in any graphene system that has zigzag edge segments.

One of the first suggestions to use the magnetic edges for spintronics applications came from Son et al. [106]. They showed that the application of a transverse electric field causes the antiferromagnetic ZGNRs to become half-metallic. Without an electric field, the system is in the antiferromagnetic ground state with a band gap at E_F . The external electric field shifts the electronic states so that the band gap of one spin component is increased while the band gap of the other spin component is closed, such that the system becomes a metal with spin-polarized electrons, i.e., a spin valve. In essence, the effect of the transverse electric field is to break the symmetry between the left and the right edge. This symmetry breaking can be achieved without an electric field in different ways, for example, by saturating the left and the right edge of the ZGNR with different functional groups [107,108] or by edge selective defects [109,110]. Other graphene-based spin-valve devices were theoretically proposed using gate-driven spin currents originating from graphene arrays doped with magnetic impurities [111,112]. An additional line of potential application targets using the phenomenon of edge magnetism in order to build a magnetoresistor [113,114]. But up to now, there is little experimental evidence for graphene edge magnetism [115,116]. Magnetic edges have never been observed in local probe microscopy; only an indirect observation has been reported recently [117].

The inability to observe magnetic edge states is supported by recent theoretical works that show that the ideal zigzag edge morphology is not very likely to exist. In fact, other nonmagnetic edge morphologies are thermodynamically much more favorable [118–120]. Furthermore, it was shown that even in perfect ZGNRs, the antiferromagnetic ground state is stable only at very low temperatures [120]. So currently, there is some evidence accumulating that the phenomenon of edge magnetism is not applicable at room temperature.

A different type of intrinsic magnetism can be induced by certain types of point defects in bulk graphene. Point defects are, for example, lattice vacancies (missing carbon atoms) [121] and chemisorbed atoms [104,122]. Similar to edges, a point defect interrupts the ideal sp^2 lattice structure and induces electronic states that can

be magnetic. Room temperature ferromagnetism was observed in proton-irradiated highly oriented pyrolytic graphite [123]. This observation was theoretically explained to come from magnetic point defects that are created by proton radiation [124].

Furthermore, magnetic properties can be induced by foreign magnetic atoms that are either adsorbed to graphene (adatoms) or replace carbon atoms in the honeycomb lattice (substitutional dopants) [124].

1.8 SYNTHESIS OF GRAPHENE

As discussed previously, the potential for graphene in materials and devices is massive. There are great expectations that this material will provide numerous socio-economic benefits. However, it is important to be aware that many of the claims being made have been made for other well-known carbon nanostructures, namely, carbon nanotubes and fullerenes. Much of the promise for these nanostructures has yet to emerge in real applications. One of the biggest bottlenecks is what on the surface seems a simple technical issue—their synthesis and formation into atomically precise structures with high degrees of reproducibility. This is particularly important for molecular electronics applications. This same difficulty also applies to graphene, and hence one of the most important areas, if not the *most* important area to address is its synthesis and manipulation. The required knowledge and understanding to provide atomically precise fabrication of this material, in a reproducible manner, that is compatible with current semiconductor technology is still lacking. Nonetheless, great strides have been made in synthesizing graphene and this is discussed in greater detail in Chapter 2. Here we simply mention the techniques used to synthesize and functionalize graphene.

By far the most common route to synthesize graphene is chemical vapor deposition (CVD). There are many CVD variations. Thermal CVD is commonly applied to graphene formation over transition metals, including copper [126–129], nickel [130–136], iridium [137–139], and ruthenium [140–144].

Thermal CVD techniques can also be used for graphene synthesis over dielectrics, namely, sapphire [145] and various other oxides [146,147]. Free-standing carbon nanosheets and planar graphite films with a few graphene layers have been successfully synthesized by plasma enhanced CVD (PECVD) [130,148,149].

A widely used technique to synthesize graphene is the thermal decomposition of hexagonal α -SiC (6H-SiC and 4H-SiC). It has the advantage that it is very clean because the epitaxially matching support crystal provides the carbon itself and no metal is involved. The technique dates back to the early 1960s when Badami found graphite on SiC by x-ray scattering after heating SiC to 2150°C in an ultrahigh vacuum (UHV) [150]. The parallel publication of the electrical response of graphene in 2004 by Novoselov et al. and Berger et al. (who used graphene grown from SiC) provided a new impetus to optimize the growth conditions of graphene on SiC [4,151].

An easy production and low-cost technique is the exfoliation of graphite. The more common exfoliation routes include mechanical exfoliation [4], ultrasound treatment in solution [152], and intercalation steps [153].

There is also an interest in producing functionalized graphene as this can open a band gap. Hydrogenation of graphene is one route. The hydrogenation changes the sp^2 structure of graphene to sp^3 hybridization. Graphene can be synthesized using a stream of hydrogen atoms [154], reactive ball milling between anthracite coal and cyclohexane [155], exchanging the fluorine in fluorinated graphite by hydrogen [156] or by dissolved metal reduction in liquid ammonia [157]. Fluorinated graphene (FG) is another proven functionalization route. There are different methods to produce FG, namely the extraction of single layers of FG from commercially available fluorinated graphite [5], the exposure of graphene to fluorine gas at $\sim 500^\circ\text{C}$ [158], placing graphene in a fluorine-based plasma [159], or exposure to xenon difluoride [160].

1.9 GRAPHENE AND SOME OF ITS APPLICATIONS

In this review, we surveyed a vast literature about graphene's unique physical properties and the main experimental techniques used to synthesize them. The multitude of topics addressed in this review attests to the prominent potential that this material has to transform the actual nanotechnology landscape with promising applications [161]. The interest in graphene has mobilized both academic and industry realms making it an ideal candidate for the design of modern nanoscale transistors, chemical and biosensors, flexible and organic light-emitting diodes (OLEDs) displays, solar and fuel cells, and other innovations. The restricted graphene mass-production and limited reproducibility in device performances are still important matters that researchers should consider in order to push graphene-based technology into a commercial status. However, the fast development of graphene research leaves no doubt that this material will revolutionize several markets such as electronics, medicine, and energy storing in the near future.

Medicine studies can also benefit from graphene's amazing properties. In particular, graphene possesses great sensorial response to external analytes, enabling the design of nanosensors to diagnose diseases [162]. Accurate biosensors can be created from DNA-functionalized graphene samples, which are capable of detecting external DNA genes associated with diseases [163]. Graphene can also have a huge impact in environmental monitoring applications bolstered by the design of graphene-based nanoscale gas sensors [164–166].

Another attractive innovation based on graphene materials reaches the electronics scope where researchers have been able to develop bendable transparent and conductive membranes composed of graphene for engineering flexible-panel displays [167]. Recent studies have revealed that graphene-based OLEDs can even top the performance of indium tin oxide (ITO) compounds, commonly used in transparent conductive electrodes [129]. Graphene is also considered to be the basis of future computing chips after the successful realization of high-speed graphene-based transistors operating at outstanding cutoff frequencies of 700–1400 GHz [168].

All these important innovations, which were generated after the first isolation of graphene layers, indicate that the use of these materials is not limited to providing simply a theoretical model that can describe the physical properties of several organic nanostructures. Graphene is occupying a centerpiece position in many scientific advances that can change our way of making and using technology. As

mentioned by A.K. Geim, we are witnessing a scientific excitement similar to the one experienced around 100 years ago with the discovery of polymers that recently supplied our lives with plastics. We expect that the innovations resulting from graphene will prove even more exciting.

REFERENCES

1. Peierls, R. 1935. Quelques propriétés typiques des corps solides. *Annales d'Institut Henri Poincaré* 5: 177.
2. Landau, L. 1937. Zur Theorie der Phasenumwandlungen II. *Physikalische Zeitschrift Sowjetunion* 11: 26.
3. Mermin, N. D. 1968. Crystalline order in two dimensions. *Physical Review* 176: 250.
4. Novoselov, K. S., Geim, A. K., Morozov, S. V., Jiang, D., Zhang, Y., Dubonos, S. V., Grigorieva, I. V., and Firsov, A. A. 2004. Electric field effect in atomically thin carbon films. *Science* 306: 666.
5. Novoselov, K. S., Geim, A. K., Morozov, S. V., Jiang, D., Katsnelson, M. I., Grigorieva, I. V., Dubonos, S. V., and Firsov, A. A. 2005. Two-dimensional gas of massless Dirac fermions in graphene. *Nature* 438: 197–200.
6. Lin, Y.-M., Dimitrakopoulos, C., Jenkins, K. A., Farmer, D. B., Chiu, H.-Y., Grill, A., and Avouris, Ph. 2010. 100-GHz transistors from water-scale epitaxial graphene. *Science* 327: 662.
7. Kim, K. S., Zhao, Y., Jang, H., Lee, S. Y., Kim, J. M., Kim, K. S., Ahn, J.-H., Kim, P., Choi, J.-Y., and Hong, B. H. 2009. Large-scale pattern growth of graphene films for stretchable transparent electrodes. *Nature* 457: 706–710.
8. De Arco, L. G., Zhang, Y., Schlenker, C. W., Ryu, K., Thompson, M. E., and Zhou, C. 2010. Continuous, highly flexible, and transparent graphene films by chemical vapor deposition for organic photovoltaics. *ACS Nano* 4: 2865.
9. Yang, N., Zhai, J., Wang, D., Chen, Y., and Jiang, L. 2010. Two-dimensional graphene bridges enhanced photo-induced charge transport in dye-sensitized solar cells. *ACS Nano* 4: 887.
10. Wallace, P. R. 1947. The band theory of graphene. *Physical Review* 71: 662.
11. Dubois, S. M.-M., Zanolli, Z., Declerck, X., and Charlier, J.-C. 2009. Electronic properties and quantum transport in graphene-based nanostructures. *The European Physical Journal B* doi: 10.1140/epjb/e2009-00327-8.
12. Hobson, J. B., and Nierenberg, W. A. 1953. The statistics of a two-dimensional, hexagonal net. *Physical Review* 89: 662.
13. Power, S. R., and Ferreira, M. S. 2010. Graphene electrons beyond the linear dispersion regime. arXiv: 1010.0908v2.
14. Morozov, S. V., Novoselov, K. S., Katsnelson, M. I., Schedin, F., Ponomarenko, L. A., Jiang, D., and Geim, A. K. 2006. Strong suppression of weak localization in graphene. *Physical Review Letters* 97: 016801.
15. Horsell, D. W., Tikhonenko, F. V., Gorbachev, R. V., and Savchenko, A. K. 2008. Weak localization in monolayer and bilayer graphene. *Philosophical Transactions of the Royal Society A* 366: 245.
16. Konstantinova, E., Dantas, S. O., and Barone, P. M. V. B. 2006. Electronic and elastic properties of two-dimensional carbon planes. *Physical Review B* 74: 035417.
17. Reich, S., Maultzsch, J., Ordejón, P., and Thomsen, C. 2002. Tight-binding description of graphene. *Physical Review B* 66: 035412.
18. Ohta, T., Bostwick, A., Seyller, T., Horn, K., and Rotenberg, E. 2006. Controlling the electronic structure of bilayer graphene. *Science* 313: 951.

19. Feldman, B. E., Martin, J., and Yacoby, A. 2009. Broken-symmetry states and divergent resistance in suspended bilayer graphene. *Nature Physics* 5: 889–983.
20. González, J. W., Santos, H., Pacheco, M., Chico, L., and Brey, L. 2010. Electronic transport through bilayer graphene. *Physical Review B* 81 (2010): 195406.
21. Melinda, Y. H., Barbaros, O., Zhang, Y., and Kim, P. 2007. Energy band-gap engineering of graphene nanoribbons. *Physical Review Letters* 98: 206805.
22. Nakada, K., Fujita, M., Dresselhaus, G., and Dresselhaus, M. S. 1996. Edge state in graphene ribbons: Nanometer size effect and edge shape dependence. *Physical Review B* 54: 17954.
23. Chen, Z. H., Lin, Y. M., Rooks, M. J., and Avouris, P. 2007. Graphene nano-ribbon electronics. *Physica E* 40: 228.
24. Han, M. Y., Ozyilmaz, B., Zhang, Y. B., and Kim, P. 2007. Energy band-gap engineering of graphene nanoribbons. *Physical Review Letters* 98: 206805.
25. Li, X., Wang, X., Zhang, L., Lee, S., and Dai, H. 2008. Chemically derived, ultrasmooth graphene nanoribbon semiconductors. *Science* 319: 1229–1233.
26. Kosynkin, D. V., Higginbotham, A. L., Sinitskii, A., Lomeda, J. R., Dimiev, A., Price, B. K., and Tour, J. M. 2009. Longitudinal unzipping of carbon nanotubes to form graphene nanoribbons. *Nature* 458: 872–877.
27. Elas, A. L., Botello-Mendez, A. R., Meneses-Rodriguez, D., Gonzalez, V. J., Ramirez-Gonzalez, D., Ci, L., Munoz-Sandoval, E., Ajayan, P. M., Terrones, H., and Terrones, M. 2009. Longitudinal cutting of pure and doped carbon nanotubes to form graphitic nanoribbons using metal clusters as nanoscalpels. *Nano Letters* 10: 366.
28. Santos, H., Chico, L., and Brey, L. 2009. Carbon nanoelectronics: Unzipping tubes into graphene ribbons. *Physical Review Letters* 103: 086801-1-4.
29. Cai, J., Ruffieux, P., Jaafar, R., Bieri, M., Braun, T., Blankenburg, S., Muoth, M., Seitsonen, A. P., Saleh, M., Feng, X., Müllen, K., and Fasel, R. 2010. Atomically precise bottom-up fabrication of graphene nanoribbons. *Nature* 466: 470.
30. Nemeč, N. Quantum transport in carbon-based nanostructures. Dr. rer. nat. (equiv. PhD) thesis, University of Regensburg, September (2007).
31. Niimi, Y., Matsui, T., Kambara, H., Tagami, K., Tsukada, M., and Fukuyama, H. 2005. Scanning tunneling microscopy and spectroscopy studies of graphite edges. *Applied Surface Science* 241: 43.
32. Son, Y.-W., Cohen, M. L., and Louie, S. G. 2006. Energy gaps in graphene nanoribbons. *Physical Review Letters* 97: 216803.
33. Rosales, L., Pacheco, M., Barticevic, Z., Leon, A., Latge, A., and Orellana, P. A. 2009. Transport properties of antidote superlattices of graphene nanoribbons. *Physical Review B* 80: 073402-1-4.
34. Ritter, C., Pacheco, M., Orellana, P., and Latge, A. 2009. Electron transport in quantum antidots made of four-terminal graphene ribbons. *Journal of Applied Physics* 106: 104303-1-6.
35. Cresti, A., and Roche, S. 2009. Edge-disorder-dependent transport length scales in graphene nanoribbons: From Klein defects to the superlattice limit. *Physical Review B* 79: 233404-1-4.
36. Jia, X., Hofmann, M., Meunier, V., Sumpter, B. G., Campos-Delgado, J., Romo-Herrera, J. M., Son, H., Hsieh, Y.-P., Reina, A., Kong, J., Terrones, M., and Dresselhaus, M. S. 2009. Controlled formation of sharp zigzag and armchair edges in graphitic nanoribbons. *Science* 323: 1701.
37. Kobayashi, Y., Fukui, K.-i., Enoki, T., Kusakabe, K., and Kaburagi, Y. 2005. Observation of zigzag and armchair edges using scanning tunneling microscopy and spectroscopy. *Physical Review B* 71: 193406.

38. Niimi, Y., Matsui, T., Kambara, H., Tagami, K., Tsukada, M., and Fukuyama, H. 2006. Scanning tunneling microscopy and spectroscopy of the electronic local density of states of graphite surfaces. *Physical Review B* 73: 085421.
39. Ihn, T., Cuettinger, J., Molitor, F., Schnez, S., Schurtenberger, E., Jacobsen, A., Hellmueller, S., Frey, T., Droescher, S., Stampfer, C., and Ensslin, K. 2010. Graphene single-electron transistors. *Materials Today* 13: 44.
40. Evaldsson, M., Zozoulenko, I. V., Xu, H., and Heinzl, T. 2008. Edge-disorder-induced Anderson localization and conduction gap in graphene nanoribbons. *Physical Review B* 78: 161407R.
41. Mucciolo, E. R., Castro Neto, A. H., and Lewenkopf, C. H. 2009. Conductance quantization and transport gaps in disordered graphene nanoribbons. *Physical Review B* 79: 075407.
42. Klein, D. J. 1994. Graphitic polymer strips with edge states. *Chemical Physics Letters* 217: 261.
43. Klein, D. J., and Bytautas, L. 1999. Graphitic edges and unpaired π -electron spins. *Journal of Physical Chemistry A* 103: 5196.
44. Areshkin, D., Gunlycke, D., and White, C. T. 2007. Ballistic transport in graphene nanostripes in the presence of disorder: Importance of edge effects. *Nano Letters* 7: 204.
45. Gunlycke, D., Areshkin, D., and White, C. T. 2007. Semiconducting graphene nanostripes with edge disorder. *Applied Physics Letters* 90: 142104.
46. Querlioz, D., Apertet, Y., Valentin, A., Huet, K., Bournel, A., Galdin-Retailleau, S., and Dollfus, P. 2008. Suppression of the orientation effects on bandgap graphene nanoribbons in the presence of edge disorder. *Applied Physics Letters* 92: 042108.
47. Rosales, L., Pacheco, M., Barticevic, Z., Latge, A., and Orellana, P. A. 2009. Conductance gaps in graphene nanoribbons designed by molecular aggregations. *Nanotechnology* 20: 095705-1-6.
48. Power, S. R., de Menezes, V. M., Fagan, S. B., and Ferreira, M. S. 2009. Model of impurity segregation in graphene nanoribbons. *Physical Review B* 80: 235424-1-5.
49. Balandin, A. A., Ghosh, S., Bao, W., Calizo, I., Teweldebrhan, D., Miao, F., and Lau, C. N. 2008. Superior thermal conductivity of single-layer graphene. *Nano Letters* 8: 902-907.
50. Seol, J. H., Jo, I., Moore, A. L., Lindsay, L., Aitken, Z. H., Pettes, M. T., Li, X., Yao, Z., Huang, R., Broido, D., Mingo, N., Ruoff, R. S., and Shi, L. 2010. Two-dimensional phonon transport in supported graphene. *Science* 328: 213-216.
51. Saito, K., Nakamura, J., and Natori, A. 2007. Ballistic thermal conductance of a graphene sheet. *Physical Review B* 76 (2007): 115409-1-4.
52. Ghosh, S., Bao, W., Nika, D. L., Subrina, S., Pokatilov, E. P., Lau, C. N., and Balandin, A. A. 2010. Dimensional crossover of thermal transport in few-layer graphene. *Nature Materials* 9: 555-558.
53. Ghosh, S., Calizo, I., Teweldebrhan, D., Pokatilov, E. P., Nika, D. L., Balandin, A. A., Bao, W., Miao, F., and Lau, C. N. 2008. Extremely high thermal conductivity of graphene: Prospects for thermal management applications in nanoelectronic circuits. *Applied Physics Letters* 92: 151911-1-3.
54. Meyer, J. C., Geim, A. K., Katsnelson, M. I., Novoselov, K. S., Booth, T. J., and Roth, S. 2007. The structure of suspended graphene sheets. *Nature* 446: 60-3.
55. Lindsay, L., Broido, D. A., and Mingo, N. 2010. Flexural phonons and thermal transport in graphene. *Physical Review B* 82: 115427-1-6.
56. Faugeras, C., Faugeras, B., Orlita, M., Potemski, M., Nair, R. R., and Geim, A. K. 2010. Thermal conductivity of graphene in corbino membrane geometry. *ACS Nano* 4: 1889-1892.

57. Cai, W., Moore, A. L., Zhu, Y., Li, X., Chen, S., Shi, L., and Ruoff, R. S. 2010. Thermal transport in suspended and supported monolayer graphene grown by chemical vapor deposition. *Nano Letters* 10: 1645–1651.
58. Seol, J. H., Moore, A. L., Shi, L., Jo, I., and Yao, Z. 2011. Thermal conductivity measurement of graphene exfoliated on silicon dioxide. *Journal of Heat Transfer* 133: 022403-1-7.
59. Jang, W., Chen, Z., Bao, W., Lau, C. N., and Dames, C. 2010. Thickness-dependent thermal conductivity of encased graphene and ultrathin graphite. *Nano Letters* 10: 3909–3913.
60. Yamamoto, T., Watanabe, K., and Mii, K. 2004. Empirical-potential study of phonon transport in graphitic ribbons. *Physical Review B* 70: 245402-1-7.
61. Gillen, R., Mohr, M., Thomsen, C., and Maultzsch, J. 2009. Vibrational properties of graphene nanoribbons by first-principles calculations. *Physical Review B* 80: 155418-1-9.
62. Munoz, E., Lu, J., and Yakobson, B. I. 2010. Ballistic thermal conductance of graphene ribbons. *Nano Letters* 10: 1652–1656.
63. Sevincli, H., and Cuniberti, G. 2010. Enhanced thermoelectric figure of merit in edge-disordered zigzag graphene nanoribbons. *Physical Review B* 81: 113401-1-4.
64. Li, W., Sevincli, H., Cuniberti, G., and Roche, S. 2010. Phonon transport in large-scale carbon-based disordered materials: Implementation of an efficient order-N and real-space Kubo methodology. *Physical Review B* 82: 041410-1-4.
65. Murali, R., Yang, Y., Brenner, K., Beck, T., and Meindl, J. D. 2009. Breakdown current density of graphene nanoribbons. *Applied Physics Letters* 94: 243114-1-3.
66. Wirtz, L., and Rubio, A. 2004. The phonon dispersion of graphite revisited. *Solid State Communications* 131: 141–152.
67. Lee, C., Wei, X., Kysar, J. W., and Hone, J. 2008. Measurement of elastic properties and intrinsic strength of monolayer graphene. *Science* 321: 385.
68. Ni, Z. H., Wang, H. M., Ma, Y., Kasim, J., Wu, Y. H., and Shen, Z. X. 2008. Tunable stress and controlled thickness modification in graphene by annealing. *ACS Nano* 2: 1033; Ni, Z. H., Yu, T., Lu, Y. H., Wang, Y. Y., Feng, Y. P., and Shen, Z. X. 2008. Uniaxial strain on graphene: Raman spectroscopy study and band-gap opening. *ACS Nano* 2: 2301.
69. Liu, F., Ming, P., and Li, J. 2007. Ab initio calculation of ideal strength and phonon instability of graphene under tension. *Physical Review B* 76: 064120.
70. Pereira, V. M., Peres, N. M. R., and Castro Neto, A. H. 2009. Tight-binding approach to uniaxial strain in graphene. *Physical Review B* 80: 045401; Pereira, V. M., and Castro Neto, A. H. 2009. Strain engineering of graphene's electronic structure. *Physical Review Letters* 103: 046801.
71. Gao, Y., and Hao, P. 2009. Mechanical properties of monolayer graphene under tensile and compressive loading. *Physica E* 41: 1561.
72. Xu, Z. 2009. Graphene nanoribbons under tension. *Journal of Computational and Theoretical Nanoscience* 6: 625.
73. Scarpa, F., Adhikari, S., and Srikantha Phani, A. 2009. Effective elastic mechanical properties of single layer graphene sheets. *Nanotechnology* 20: 065709.
74. Lu, Q., and Huang, R. 2010. Effect of edge structures on elastic modulus and fracture of graphene nanoribbons under uniaxial tension. arXiv: 1007.3298.
75. Mohiuddin, T. M. G., Lombardo, A., Nair, R. R., Bonetti, A., Savini, G., Jalil, R., Bonini, N., Basko, D. M., Galiotis, C., Marzari, N., Novoselov, K. S., Geim, A. K., and Ferrari, A. C. 2009. Uniaxial strain in graphene by Raman spectroscopy: G peak splitting, Grueneisen parameters, and sample orientation. *Physical Review B* 79: 205433-1-8.
76. Huang, M., Yan, H., Chen, C., Song, D., Heinz, T. F., and Hone, J. 2009. Phonon softening and crystallographic orientation of strained graphene studied by Raman spectroscopy. *Proceedings of the National Academy of Sciences USA* 106: 7304–7308.

77. Poetschke, M., Rocha, C. G., Foa Torres, L. E. F., Roche, S., and Cuniberti, G. 2010. Modeling graphene-based nanoelectromechanical devices. *Physical Review B* 81: 193404-1-4.
78. Erdogan, E., Popov, I., Rocha, C. G., Cuniberti, G., Roche, S., and Seifert, G. 2011. Engineering carbon chains from mechanically stretched graphene-based materials. *Physical Review B* 83: 041401(R).
79. Hod, O., and Scuseria, G. E. 2009. Electromechanical properties of suspended graphene nanoribbons. *Nano Letters* 9: 2619–2622.
80. Topsakal, M., and Ciraci, S. 2010. Elastic and plastic deformation of graphene, silicene, and boron nitride honeycomb nanoribbons under uniaxial tension: A first-principles density-functional theory study. *Physical Review B* 81: 024107-1-6.
81. Topsakal, M., Bagci, V. M. K., and Ciraci, S. 2010. Current-voltage (I-V) characteristics of armchair graphene nanoribbons under uniaxial strain. *Physical Review B* 81: 205437-1-5.
82. Isacsson, A. 2010. Nanomechanical displacement detection using coherent transport in ordered and disordered graphene nanoribbon resonators. arXiv: 1010.0508v1.
83. Ho, J. H., Chiu, Y. H., Tsai, S. J., and Lin, M. F. 2009. Semimetallic graphene in a modulated electric field. *Physical Review B* 79: 115427.
84. Novikov, D. S. 2007. Transverse field effect in graphene ribbons. *Physical Review Letters* 99: 056802.
85. Raza, H., and Kan, E. C. 2008. Armchair graphene nanoribbons: Electronic structure and electric-field modulation. *Physical Review B* 77: 245434.
86. Kan, E.-J., Li, Z., Yang, J., and Hou, J. G. 2007. Will zigzag graphene nanoribbon turn half metal under electric field? *Applied Physics Letters* 91: 243116.
87. Kinder, J. M., Dorando, J. J., Wang, H., and Chan, G. K.-L. 2009. Perfect reflection of chiral fermions in gated graphene nanoribbons. *Nano Letters* 9: 1980–1983.
88. Yu, Y.-J., Zhao, Y., Louis, S. R., Kwang, E. B., Kim, S., and Kim, P., 2009. Tuning the graphene work function by electric fields. *Nano Letters* 9: 3430–3434.
89. Yan, J., Zhang, Y., Kim, P., and Pinczuk, A. 2007. Electric field effect tuning electron-phonon coupling in graphene. *Physical Review Letters* 98: 166802.
90. Wang, Z. 2009. Alignment of graphene nanoribbons by an electric field. *Carbon* 47: 3050–3053.
91. Dalosto, S. D., and Levine, Z. H. 2008. Controlling the band gap in zigzag graphene nanoribbons with an electric field induced by a polar molecule. *Journal of Physical Chemistry C* 112: 8196–8199.
92. Ritter, C., Makler, S. S., and Latgé, A. 2008. Energy-gap modulations of graphene nanoribbons under external fields: A theoretical study. *Physical Review B* 77: 195443-1-5.; *Physical Review B* 82: 089903-1-2.
93. Chen, S. C., Wang, T. S., Lee, C. H., and Lin, M. F. 2008. Magneto-electronic properties of graphene nanoribbons in the spatially modulated electric field. *Physics Letters A* 372: 5999–6002.
94. Ho, J. H., Lai, Y. H., Lu, C. L., Hwang, J. S., Chang, C. P., and Lin, M. F. 2006. Electronic structure of a monolayer graphite layer in a modulated electric field. *Physics Letters A* 359: 70–75.
95. Lukose, V., Shankar, R., and Baskaran, G. 2007. Novel electric field effects on Landau levels in graphene. *Physical Review Letters* 98: 116802-1-4.
96. Zhang, S., Ma, N., and Zhang, E. 2010. The modulation of the Haas-van Alphen effect in graphene by electric field. *Journal of Physics: Condensed Matter* 22: 115302-1-8.
97. Kohler, S., Lehmann, J., and Haenggi, P. 2005. Driven quantum transport on the nanoscale. *Physics Reports* 406: 379–443.
98. Foa Torres, L. E. F., and Cuniberti, G. 2009. Controlling the conductance and noise of driven carbon-based Fabry-Perot devices. *Applied Physics Letters* 94: 222103-1-3.

99. Zhu, R., and Chen, H. 2009. Quantum pumping with adiabatically modulated barriers in graphene. *Applied Physics Letters* 95: 122111-1-3.
100. Prada, E., San-Jose, P., and Schomerus, H. 2009. Quantum pumping in graphene. *Physical Review B* 80: 245414-1-5.
101. Rocha, C. G., Foa Torres, L. E. F., and Cuniberti, G. 2010. Ac transport in graphene-based Fabry-Pérot devices. *Physical Review B* 81: 115435-1-8.
102. Oka, T., and Aoki, H. 2009. Photovoltaic Hall effect in graphene. *Physical Review B* 79: 081406-1-4.
103. Fujita, M., Wakabayashi, K., Nakada, K., and Kusakabe, K. 1996. Peculiar localized state at zigzag graphite edge. *Journal of the Physical Society of Japan* 65:1920-1-4.
104. Yazyev, O. V. 2010. Emergence of magnetism in graphene materials and nanostructures. *Reports on Progress in Physics* 73:056501-1-16.
105. Lieb, E. H. 1989. Two theorems on the Hubbard model. *Physical Review Letters* 62:1201-1-4.
106. Son, Y.-W. Cohen, M. L., and Louie, S. G. 2006. Half-metallic graphene nanoribbons. *Nature* 444:347-1-3.
107. Kan, E.-J., Li, Z., Yang, J., and Hou, J. G. 2008. Half-metallicity in edge-modified zigzag graphene nanoribbons. *Journal of the American Chemical Society* 130:4224-1-2.
108. Cantele, G., Lee, Y.-S., Ninno, D., and Marzari, N. 2009. Spin channels in functionalized graphene nanoribbons. *Nano Letters* 9:3425-1-4.
109. Wimmer, M., Adagideli, I., Berber, S., Tománek, D., and Richter, K. 2008. Spin currents in rough graphene nanoribbons: Universal fluctuations and spin injection. *Physical Review Letters* 100:177207-1-4.
110. Lakshmi, S., Roche, S., and Cuniberti, G., 2009. Spin valve effect in zigzag graphene nanoribbons by defect engineering. *Physical Review B* 80:193404-1-4.
111. Guimaraes, F. S. M., Costa, A. T., Muniz, R. B., and Ferreira, M. S. 2010. Graphene-based spin-pumping transistor. *Physical Review B* 81: 233402-1-4.
112. Guimaraes, F. S. M., Costa, A. T., Muniz, R. B., and Ferreira, M. S. 2010. Graphene as a non-magnetic spin-current lens. arXiv: 1009.6228v1.
113. Kim, W. Y., and Kim, K. S. 2008. Prediction of very large values of magnetoresistance in a graphene nanoribbon device. *Nature Nanotechnology* 3:408-1-5.
114. Muñoz-Rojas, F., Fernández-Rossier, J., and Palacios, J. J. 2009. Giant magnetoresistance in ultrasmall graphene-based devices. *Physical Review Letters* 102:136810-1-4.
115. Sepioni, M., Nair, R. R., Rablen, S., Narayanan, J., Tuna, F., Winpenny, R., Geim, A. K., and Grigorieva, I. V. 2010. Limits on intrinsic magnetism in graphene. *Physical Review Letters* 105:207205-1-4.
116. Mermin, N. D., and Wagner, H. 1966. Absence of ferromagnetism or antiferromagnetism in one- or two-dimensional isotropic Heisenberg models. *Physical Review Letters* 17:1133-1-4.
117. Joly, V. L. J., Kiguchi, M., Hao, S.-J., Takai, K., Enoki, T., Sumii, R., Amemiya, K., Muramatsu, H., Hayashi, T., Kim, Y. A., Endo, M., Campos-Delgado, J., López-Urfas, F., Botello-Méndez, A., Terrones, H., Terrones, M., and Dresselhaus, M. S. 2010. Observation of magnetic edge state in graphene nanoribbons. *Physical Review B* 81:245428-1-6.
118. Wassmann, T., Seitsonen, A. P., Saitta, A. M., Lazzeri, M., and Mauri, F. 2008. Structure, stability, edge states, and aromaticity of graphene ribbons. *Physical Review Letters* 101:096402-1-4.
119. Koskinen, P., Malola, S., and Häkkinen, H. 2008. Self-passivating edge reconstructions of graphene. *Physical Review Letters* 101:115502-1-4.
120. Kunstmann, J., Özdoğan, C., Quandt, A., and Fehske, H. 2011. Stability of edge states and edge magnetism in graphene nanoribbons. *Physical Review B* 83:045414-1-8.
121. Lehtinen, P. O., Foster, A. S., Ma, Y., Krashennnikov, A., and Nieminen, R. M. 2004. Irradiation-induced magnetism in graphite: A density functional study. *Physical Review Letters* 93:1872021-1-4.

122. Duplock, E. J., Scheffler, M., and Lindan, P. J. D. 2004. Hallmark of perfect graphene. *Physical Review Letters* 92:225502-1-4.
123. Esquinazi, P., Spemann, D., Höhne, R., Setzer, A., Han, K. H., and Butz, T. 2003. Induced magnetic ordering by proton irradiation in graphite. *Physical Review Letters* 91:227201-1-4.
124. Yazyev, O. V. 2008. Magnetism in disordered graphene and irradiated graphite. *Physical Review Letters* 101:037203-1-4.
125. Sevinçli, H., Topsakal, M., Durgun, E., and Ciraci, S. Electronic and magnetic properties of 3D transition-metal atom adsorbed graphene and graphene nanoribbons. *Physical Review B* 77:195434.
126. Li, X., Cai, W., An, J., Kim, S., Nah, J., Yang, D., Piner, R., Velamakanni, A., Jung, I., Tutuc, E., Banerjee, S. K., Colombo, L., and Ruoff, R. S. 2009. Large-area synthesis of high-quality and uniform graphene films on copper foils. *Science* 324: 1312–1314.
127. Li, X., Magnuson, C. W., Venugopal, A., An, J., Suk, J. W., Han, B., Borysiak, M., Cai, W., Velamakanni, A., Zhu, Y., Fu, L., Vogel, E. M., Voelkl, E., Colombo, L. and Ruoff, R. S. 2010. Graphene films with large domain size by a two-step chemical vapor deposition process. *Nano Letters* 10(11):4328–4334.
128. Hamilton, J. C., and Blakely, J. M. 1980. Carbon segregation to single crystal surfaces of Pt, Pd and Co. *Surface Science* 91(1): 199–218.
129. Wu, W., Liu, Z., Jauregui, L. A., Yua, Q., Pillai, R., Cao, H., Bao, J., Chen, Y. P., and Pei, S.-S. 2010. Wafer-scale synthesis of graphene by chemical vapor deposition and its application in hydrogen sensing. *Sensors and Actuators B* 150: 296–300.
130. Obratsova, A. N., Obratsova, E. A., Tyurnina, A. V., and Zolotukhin, A. A. 2007. Chemical vapor deposition of thin graphite films of nanometer thickness. *Carbon* 45: 2017–2021.
131. Yu, Q., Lian, J., Siriponglert, S., Li, H., Chen, Y. P., and Pei, S.-S. 2008. Graphene segregated on Ni surfaces and transferred to insulators. *Applied Physics Letters* 93: 113103-1-3.
132. Dedkov, Y. S., Fonin, M., Rüdiger, U., and C. Laubschat. 2008. Rashba effect in the graphene/Ni(111) system. *Physical Review Letters* 100: 107602-1-4.
133. Fuentes-Cabrera, M., Baskes, M. I., Melechko, A. V., and Simpson, M. L. 2008. Bridge structure for the graphene/Ni(111) system: A first principles study. *Physical Review B* 77:035405-1-5.
134. Dedkov, Y.S., Fonin, M., Rüdiger, U., and Laubschat, C. 2008. Graphene-protected iron layer on Ni(111). *Applied Physics Letters* 93: 022509-1-3.
135. Usachov, D., Dobrotvorskiy, A.M., Varykhalov, A., Rader, O., Gudat, W., Shikin, A. M., and Adamchuk, V. K. 2008. Experimental and theoretical study of the morphology of commensurate and incommensurate graphene layers on Ni single-crystal surfaces. *Physical Review B* 78: 085403-1-8.
136. Varykhalov, A., Sánchez-Barriga, J., Shikin, A. M., Biswas, C., Vescovo, E., Rybkin, A., Marchenko, D., and Rader, O. 2008. Electronic and magnetic properties of quasi-freestanding graphene on Ni. *Physical Review Letters* 101:157601-1-4.
137. Coraux, J., N'Diaye, A. T., Busse, C., and Michely, T. 2008. Structural coherency of graphene on Ir(111). *Nano Letters* 8 (2): 565–570.
138. Preobrajenski, A. B., Ng, M. L., Vinogradov, A. S., and N. Mårtensson, N. 2008. Controlling graphene corrugation on lattice-mismatched substrates. *Physical Review B* 78: 073401-1-4.
139. Pletikosić, I., Kralj, M., Pervan, P., Brako, R., Coraux, J., N'Diaye, A. T., Busse, C., and Michely, T. 2009. Dirac cones and minigaps for graphene on Ir(111). *Physical Review Letters* 102: 056808-1-4.
140. Yi, P., Dong-Xia, S., and Hong-Jun, G. 2007. Formation of graphene on Ru(0001] surface. *Chinese Physics* 16 (11): 3151–3153.

141. Sutter, P. W., Flege, J.-I., and Sutter, E. A. 2008. Epitaxial graphene on ruthenium. *Nature Materials* 7:406–411.
142. Marchini, S., Günther, S., and Winterlin, J. 2007. Scanning tunneling microscopy of graphene on Ru(0001). *Physical Review B* 76:075429-1-9.
143. Vázquez de Parga, A. L., Calleja, F., Borca, B., Passeggi, M. C. J., Hinarejos, J. J., Guinea, F., and Miranda, R. 2008. Periodically rippled graphene: Growth and spatially resolved electronic structure. *Physical Review Letters* 100:056807-1-4.
144. Jiang, D.-E., Du, M.-H., and Dai, S. 2009. First principles study of the graphene/Ru(0001) interface. *Journal of Chemical Physics* 130:074705-1-5.
145. Hwang, J., Shields, V. B., Thomas, C. I., Shiraraman, S., Hao, D., Kim, M., Woll, A. R., Tompa, G. S., and Spencer, M. G. 2010. Epitaxial growth of graphitic carbon on C-face SiC and sapphire by chemical vapor deposition (CVD). *Journal of Crystal Growth* 312:3219–3224.
146. Rümmeli, M. H., Kramberger, C., Grüneis, A., Ayala, P., Gemming, T., Büchner, B., and Pichler, T. 2007. On the graphitization nature of oxides for the formation of carbon nanostructures. *Chemistry of Materials* 19(17):4105–4107.
147. Rümmeli, M. H., Bachmatiuk, A., Scott, A., Börrnert, F., Warner, J. H., Hoffman, V., Lin, J.-H., Cuniberti, G., and Büchner, B. 2010. Direct low-temperature nanographene CVD synthesis over a dielectric insulator. *ACS Nano* 4(7):4206–4210.
148. Wang, J. J., Zhu, M. Y., Outlaw, R. A., Zhao, X., Manos, D. M., Holloway, B. C., and Mammanna, V. P. 2004. Free-standing subnanometer graphite sheets. *Applied Physics Letters* 85:1265–1267.
149. Somani, P. R., Somani, S. P., and Umeno, M. 2006. Planar nano-graphenes from camphor by CVD. *Chemical Physics Letters* 430: 56–59.
150. Badami, D. V. 1962. Graphitization of α -silicon carbide. *Nature* 193:569–570.
151. Berger, C., Song, Z., Li, T., Li, X., Ogbazghi, A. Y., Feng, R., Dai, Z., Marchenkov, A. N., Conrad, E. H., First, P. N., and de Heer, W. A. 2004. Ultrathin epitaxial graphite: 2D electron gas properties and a route toward graphene-based nanoelectronics. *Journal of Chemical Physics* 120:11931–11936.
152. Hernandez, Y., Nicolosi, V., Lotya, M., Blighe, F. M., Sun, Z., De, S., McGovern, I. T., Holland, B., Byrne, M., Gun'Ko, Y. K., Boland, J. J., Niraj, P., Duesberg, G., Sathesh, K., Goodhue, R., Hutchison, J., Scardaci, V., Ferrari, A. C., and Coleman, J. N. 2008. High-yield production of graphene by liquid-phase exfoliation of graphite. *Nature Nanotechnology* 3:563–568.
153. Zhu, J. 2008. New solutions to a new problem. *Nature Nanotechnology* 3:528–529.
154. Elias, D. C., Nair, R. R., Mohiuddin, T. M., Morozov, S. V., Blake, P., Halsall, M. P., Ferrari, A. C., Boukhalov, D. W., Katsnelson, M. I., Geim, A. K., and Novoselov, K. S. 2009. Control of graphene's properties by reversible hydrogenation: Evidence for graphene. *Science* 323:610-613.
155. Lueking, A. D., Gutierrez, H. R., Foneseca, D. A., Narayanan, D. L., VanEssendelft, D., Jain, P., and Clifford, C. E. B. 2006. Combined hydrogen production and storage with subsequent carbon crystallization. *Journal of American Chemical Society* 128:7758-60.
156. Sato, Y., Watano, H., Hagiwara, R., and Ito, Y. 2006. Reaction of layered carbon fluorides C_xF (x = 2.5–3.6) and hydrogen. *Carbon* 44: 664-670.
157. Pekker, S., Salvétat, J.-P., Jakab, E., Bonard, J.-M., and Forro, L. 2001. Hydrogenation of carbon nanotubes and graphite in liquid ammonia. *Journal of Physical Chemistry B* 105: 7938–7943.
158. Felten, A., Bittencourt, C., Pireaux, J. J., Van Lier, G., and Charlier, J. C. 2005. Radio-frequency plasma functionalization of carbon nanotubes surface O₂, NH₃, and CF₄ treatments. *Journal of Applied Physics* 98: 074308-5.

159. Ruff, O., Bretschneider, O., and Ebert, F. Z. 1934. Die Reaktionsprodukte der verschiedenen Kohlenstoffformen mit Fluor II (Kohlenstoff-monofluorid). *Anorg. Allgm. Chem.* 217:1–18.
160. Robinson, J. T., Burgess, J. S., Junkermeier, C. E., Badescu, S. C., Reinecke, T. L., Perkins, F. K., Zalalutdniov, M. K., Baldwin, J. W., Culbertson, J. C., Sheehan, P. E., and Snow, E. S. 2010. Properties of fluorinated graphene films. *Nano Letters* 10:3001–5.
161. van Noorden, R. 2011. The trials of new carbon. *Nature* 469:14–16.
162. Shao, Y., Wang, J., Wu, H., Liu, J., Aksay, I. A., and Lin, Y. 2010. Graphene based electrochemical sensors and biosensors: A review. *Electroanalysis* 22: 1027–1036.
163. Tang, Z., Wu, H., Cort, J. R., Buchko, G. W., Zhang, Y., Shao, Y., Aksay, I. A., Liu, J., and Lin, Y. 2010. Constraint of DNA on functionalized graphene improves its biostability and specificity. *Small* 6: 1205–1209.
164. Schedin, F., Geim, A. K., Morozov, S. V., Hill, E. W., Blake, P., Katsnelson, M. I., and Novoselov, K. S. 2007. Detection of individual gas molecules adsorbed on graphene. *Nature Materials* 6: 652–655.
165. Dan, Y., Lu, Y., Kybert, N. J., Luo, Z., and Charlie Johnson, A. T. 2009. Intrinsic response of graphene vapor sensors. *Nano Letters* 9: 1472–1475.
166. Ratinac, K. R., Yang, W., Ringer, S. P., and Braet, F. 2010. Toward ubiquitous environmental gas sensors—Capitalizing on the promise of graphene. *Environmental Science Technology* 44: 1167–1176.
167. Bae, S., Kim, H., Lee, Y., Xu, X., Park, J.-S., Zheng, Y., Balakrishnan, J., Lei, T., Kim, H. R., Song, Y. I., Kim, Y.-J., Kim, K. S., Özyilmaz, B., Ahn, J.-H., Hong, B. H., and Iijima, S. 2010. Roll-to-roll production of 30-inch graphene thin films for transparent electrodes. *Nanotechnology* 5: 574–578.
168. Liao, L., Bai, J., Cheng, R., Lin, Y.-C., Jiang, S., Qu, Y., Huang, Y., and Duan, X. 2010. Sub-100 nm channel length graphene transistors. *Nano Letters* 10: 3952–3956.